A Wearable All-Fabric Thermoelectric Generator

Linden K. Allison and Trisha L. Andrew*

Wearable thermoelectric generators are a promising energy source for powering activity trackers and portable health monitors. However, known iterations of wearable generators have large form factors, contain expensive or toxic materials with low elemental abundance, and quickly reach thermal equilibrium with a human body, meaning that thermoelectric power can only be generated over a short period of wear. Here, an all-fabric thermopile is created by vapor printing persistently *p*-doped poly(3,4-ethylenedioxythiophene) (PEDOT-Cl) onto commercial cotton and this thermopile is integrated into a specially designed, wearable band that generates thermovoltages >20 mV when worn on the hand. It is shown that the reactive vapor coating process creates mechanically rugged fabric thermopiles that yield notably high thermoelectric power factors at low temperature differentials, as compared to solution-processed counterparts. Further, best practices for naturally integrating thermopiles into garments are described, which allow for significant temperature gradients to be maintained across the thermopile despite continuous wear.

1. Introduction

Emergent wearable sensors provide a promising means for personalized health monitoring and in-home healthcare.[1] Biosensors, data transmitters, and power delivery lines have been creatively miniaturized, yet batteries and power sources remain large and bulky, ultimately limiting the functionality and broad use of portable devices.[2] The core problem is that microelectronic components require high energy densities to function, but development of portable, lightweight, low-form-factor energy harvesting, and charge storing components has been comparatively slower. Fortunately, electronic garments have access to unique power sources coming from the human body, such as small body motions and body heat, which can be harnessed to provide supplemental or backup power for microelectronic sensors.[3–5]

In theory, the thermoelectric effect can be utilized to convert radiant body heat into a source of power by taking advantage of a temperature differential between the body and cooler ambient air.[6–8] Materials with high electrical conductivities and low thermal conductivities, known as thermoelectric materials,

demonstrate the ability to produce power when exposed to a temperature gradient. The low thermal conductivity of the material prevents rapid heat equilibration, which creates an inequity of energy across the material. This disparity in energy induces the migration of charges within the material toward the colder side.[9–12]

Researchers have theorized that up to 5 mW of power can be harvested from a normal human body after an 8 h workday in an indoor environment by clipping silicon thermopiles to the outer surfaces of garments.[13] However, the form factor and garment integration of these thermopiles needs to be optimized before practical thermoelectric generators (TEGs) can be expected.[14,15] Additionally, the availability and toxicity/biocompatibility of materials must be considered when constructing a wearable device. While the most efficient thermoelectric generators are composed of Bi_2Te_3,[16–20] tellurium is a toxic, rare earth chalcogenide of limited availability.[21] Silicon-based devices do not face this hurdle but demonstrate significantly lower thermoelectric harvesting efficiencies and poor flexibility.[22]

Alternatively, conjugated polymers are biocompatible, flexible and lightweight materials comprised of earth-abundant elements, that are perfectly positioned for integration with body-worn electronics.[23] However, the observed thermoelectric performance of typical, solution-processed polymers have not matched those of inorganic counterparts to date[24,25] and, therefore, polymers have only been used as composites with higher efficiency materials, such as carbon nanotubes,[26–29] that often demonstrate attenuated or unreliable performances when incorporated into natural fibers or fabrics.[30]

In this work, we show that vapor-printed conjugated polymer films on fabrics display remarkably high thermoelectric power factors and can be incorporated into a custom-knit garment that yields high, stable thermovoltage outputs when worn on the body.

2. Results and Discussion

Vapor Coating Fabrics: A custom-built quartz wall reactor equipped with a heated crucible and a controlled inlet for monomer vapors was used to vapor print persistently *p*-doped poly(3,4-ethylenedioxythiophene) (PEDOT-Cl) onto fabrics (**Figure 1**).[31] Inside the reactor, vapor-phase polymerization selectively occurred at the meeting place of the monomer and oxidant vapors, and the exposed face of any fabrics placed

L. K. Allison, Prof. T. L. Andrew
Department of Chemistry
University of Massachusetts Amherst
Amherst, MA 01003, USA
E-mail: tandrew@umass.edu

The ORCID identification number(s) for the author(s) of this article can be found under https://doi.org/10.1002/admt.201800615.
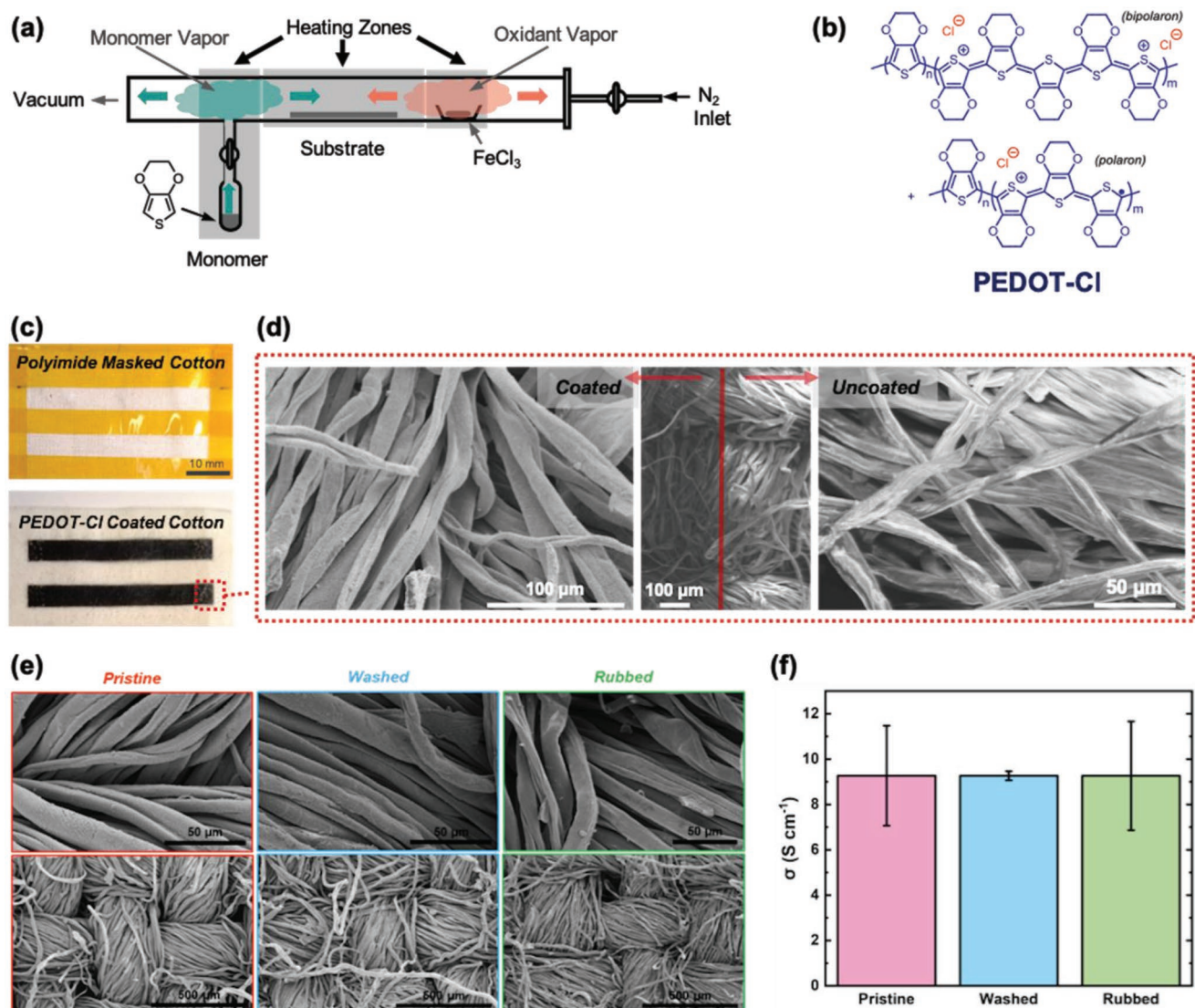
Figure 1. a) Schematic of the reactor used to vapor print conducting polymer coatings onto fabrics. b) Chemical structure of the conductive PEDOT-Cl coating. c) Standard cotton patterned with polyimide tape before and after coating with PEDOT-Cl, and d) scanning electron microscopy images (SEMs) of one edge of a PEDOT-Cl pattern, showing coated and uncoated areas. e) SEMs and f) surface electrical conductivities of PEDOT-Cl coated cotton before and after laundering or rubbing 500 times.
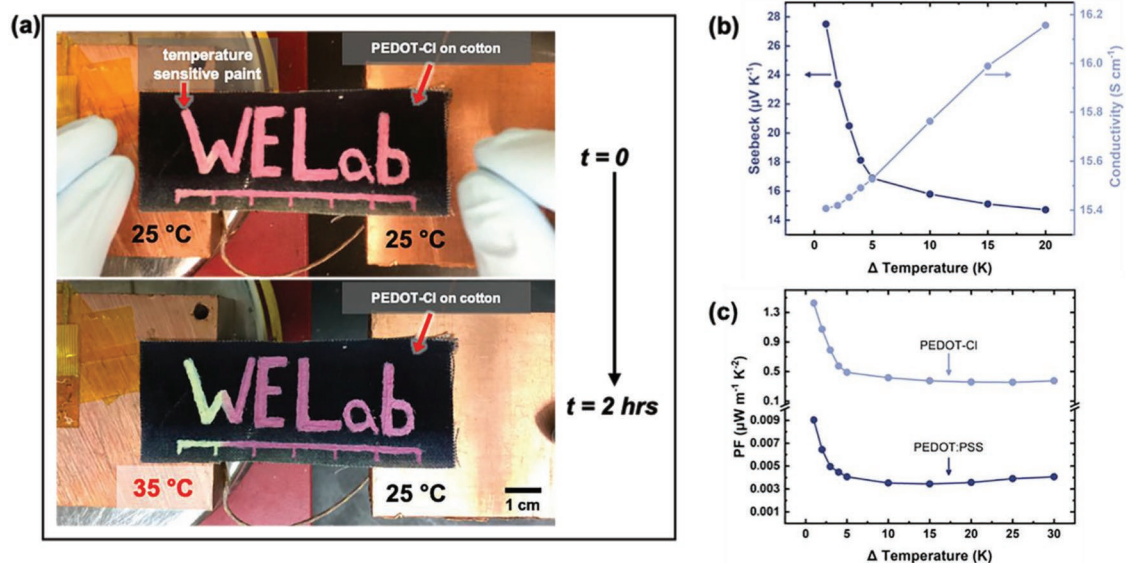
in this region was uniformly and conformally coated with PEDOT-Cl (Figure 1b).[32,33] By maintaining a reactor base pressure <200 mTorr and choosing fabrics with a medium to tight weave density, only one face of a target fabric swatch could be selectively coated, as previously described,[32] affording fabrics with one coated and one uncoated face.

Two types of cotton fabrics, standard cotton (tight weave) and tobacco cotton (medium weave), were chosen because cotton is lightweight, breathable, and widely available. Cotton fabrics are also known to possess low, weave-modulated thermal conductivity[34] and, therefore, we posited that cotton fabrics could attenuate thermal transport through the PEDOT-Cl coating when used as an underlying substrate. Patterned coatings could be easily created on cotton using contact masking. Polyimide tape was used as cost-effective contact mask that produced crisp polymer edges without leaving behind an adhesive residue

(Figure 1c,d). The thickness of the PEDOT-Cl coating was controlled by varying the duration of the vapor coating operation. Coating thickness of ≈1 µm was used for this work.

The durability of the PEDOT-Cl coating on cotton was tested by rubbing or laundering the coated fabrics in warm water. Scanning electron microscopy images (SEMs, Figure 1e) revealed that the coatings did not crack, delaminate, or mechanically wash away upon being laundered or abraded, confirming the mechanical ruggedness of the vapor-printed PEDOT-Cl (consistent with our previous work).[32]

The surface electrical conductivities of the PEDOT-Cl coatings were measured using a custom-built four-point probe. As expected, PEDOT-Cl coated tobacco cotton—the comparatively looser weave fabric—demonstrated higher electrical conductivities as compared to coated, tight-woven standard cotton (loose weaves should lead to higher surface conductivities due to

**ADVANCED
SCIENCE NEWS**

www.advancedsciencenews.com

**ADVANCED
MATERIALS
TECHNOLOGIES**

www.advmattechnol.de

Figure 2. a) Visualizing lateral (*in-plane*) heat transfer across a PEDOT-Cl coated standard cotton fabric using color-changing thermochromic paint. b) Seebeck coefficient and conductivity of PEDOT-Cl on tobacco cotton, where T_C is measure at 25 °C. c) Thermoelectric power factors of PEDOT-Cl on tobacco cotton and cotton dipdyed with PEDOT:PSS, where T_C is measure at 25 °C.
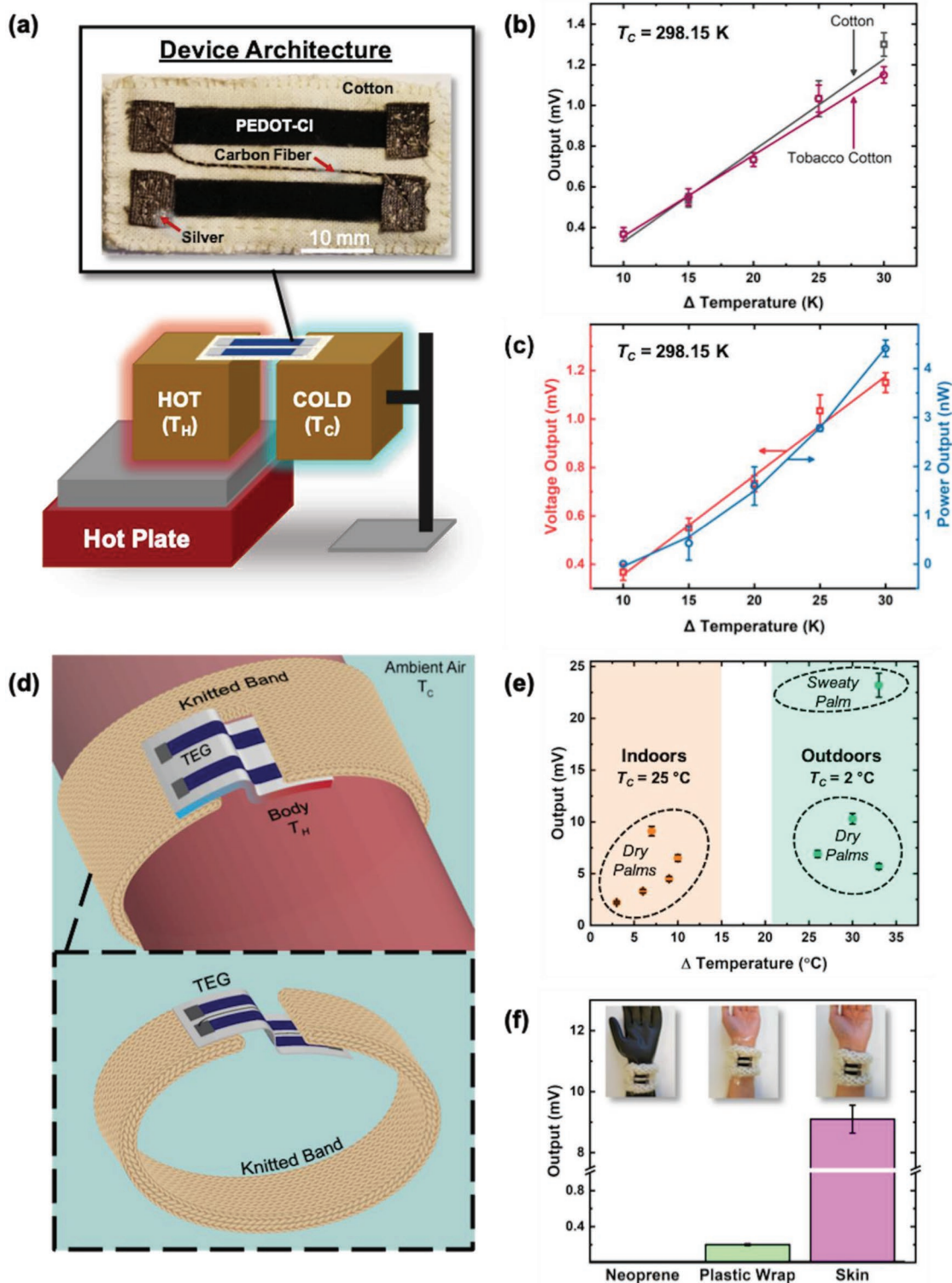
fewer physical breaks in the conductive channel[32]). Furthermore, the electrical conductivities (Figure 1f) of the PEDOT-Cl coatings on both cotton fabrics remained largely unchanged after rubbing and laundering.

Thermoelectric Efficiencies: The thermal transport properties of vapor-printed, thin conjugated polymer films have been previously characterized.[35] Here, we focused on understanding the influence of the underlying fabric on heat transport in the polymer coating. Heat transport across the length of PEDOT-Cl coated fabrics was visualized using temperature-sensitive (thermochromic) paint that changed color from red to yellow above temperatures of 30 °C (**Figure 2**). One end of a rectangular, 2.5 in. long PEDOT-Cl coated tobacco cotton swatch was placed on top of a heated copper block held at 35 °C, while the other end was placed on top of a second copper block held at 25 °C. The uncoated side of the swatch was in physical contact with the copper blocks, such that heat could only reach the top-facing PEDOT-Cl coating through the cotton. As seen in Figure 2a, the thermochromic paint on the side of the fabric that contacted the heated copper block changed color to yellow, confirming that heat was able to vertically travel from the bottom heat source, through the cotton fabric, to the top-facing PEDOT-Cl coating. Interestingly, however, the fabric swatch was observed to strictly maintain a thermal gradient laterally across its length even after hours of continuous heating. As can be seen in the movie in the Supporting Information (Movie S1), the thermochromic paint on the cold end of the fabric remained red, indicating that the temperature of this end of the swatch stayed at 25 °C and did not equilibrate over time to 35 °C. The color change in the thermochromic paint was only observed to laterally extended ≈0.5 cm beyond the end of the heat source, even after two hours of constant heating. This observation revealed that, while heat could effectively travel through porous fabrics (perpendicular to the fabric plane), in-plane thermal transport along the length of

a fabric was advantageously negligible (Figure S1, Supporting Information).

For a 1 µm thick coating of PEDOT-Cl on cotton, the measured Seebeck coefficient was 16 µV K^{-1} (Figure 2b) and the power factor was calculated to be 0.48 µW m^{-1} K^{-2} (Figure 2c). This power factor value was over two orders of magnitude greater than that of standard cotton dipdyed with PEDOT:poly(styrene sulfonic acid) (PSS) (prepared following a previously reported procedure[36]), which demonstrated a power factor of 0.0041 µW m^{-1} K^{-2} and a Seebeck coefficient of 30 µV K^{-1}. No pretreatments or chemical additives were used in the preparation of the PEDOT:PSS samples in order to provide a direct comparison with the PEDOT-Cl.

Next, all-fabric thermopiles were constructed by selectively vapor printing two rectangular PEDOT-Cl legs (p-type) on one face of either standard or tobacco cotton, and sewing one 45–50 mm-long carbon fiber thread (n-type) onto the coated face of the fabric such that opposite ends of each PEDOT-Cl leg were electrically connected together (**Figure 3**). Squares of silver-coated nylon were sewed between the carbon fiber thread and each PEDOT-Cl leg to minimize motion-induced contact drops between the carbon fiber thread and the PEDOT-Cl coating. Thermovoltage outputs from this device as a function of temperature difference were obtained using the measurement setup depicted in Figure 3a. Small operating temperatures (differentials of 30 °C maximum) were chosen in order to simulate typical temperature gradients between a human body and ambient. As seen in Figure 3b, a two-leg thermopile on standard cotton continuously produced up to 1.2 mV at a temperature difference of 30 K, even after two hours of constant heating. To place this observation in context, the champion fabric thermopile reported by Grunlan et al.[28] was comprised of five nanocomposite legs and produced a thermovoltage of 5 mV at a temperature difference of 50 K.

**ADVANCED
SCIENCE NEWS**
www.advancedsciencenews.com

**ADVANCED
MATERIALS
TECHNOLOGIES**
www.advmattechnol.de

Figure 3. a) The thermoelectric measurement setup and architecture of an all-fabric thermopile. b) Thermovoltage outputs for a standard cotton and tobacco cotton thermopile, where T_C is measure at 25 °C. c) Thermoelectric power and voltage outputs for a tobacco cotton thermopile, where T_C is measure at 25 °C. d) Design schematic of a wearable thermoelectric generator (TEG). e) Thermovoltage outputs obtained when multiple subjects wore the knit TEG on their palm. Ten TEGs were tested across twelve volunteers. ΔT is the difference between the wearer's palm and ambient air. f) Thermovoltage outputs obtained from the wearable TEG when thermal insulation layers were inserted between the subject and the TEG.

The resistivities of the PEDOT-Cl legs were separately monitored during the course of this experiment in order to determine if the polymer was thermally degrading upon heating. The PEDOT-Cl coating showed no changes in resistance throughout all measurements, which confirmed that the polymer was stable under the testing conditions and that the observed voltage outputs were solely a result of the thermoelectric effect.

Fabric weave density did not significantly impact the thermovoltage output, as two-leg thermopiles created on both standard and tobacco cotton displayed similar voltage outputs. However, the tobacco cotton device demonstrated lower surface sheet resistivities for the PEDOT-Cl leg when measured end to end (20 kΩ), as compared to the standard cotton device (150 kΩ). Due to this lower resistance, the tobacco cotton thermopile displayed a higher thermoelectric power factor: upward of 4.5 nW was generated at a temperature difference of 30 K (Figure 3c).

Thermoelectric Garments: In order to produce a wearable TEG, stretchy bands that could be worn on a wrist, palm, and upper arm were targeted, as these body parts were observed to radiate the most heat using a thermal camera (Figure S2, Supporting Information). A stretchy band was first knitted using thick wool yarn and, then, the two-leg tobacco cotton thermopile depicted in Figure 3a was sewn into the band in such a way that one half was exposed to ambient air, while the other half was buried under the knit band. When worn, the air-exposed half of the thermopile was insulated from radiant body heat by the thick yarn of the band, whereas the buried half contacted the body (with warm "still air"[37] trapped between the body and the thermopile) and equilibrated to body temperature. Only the uncoated face of thermopile came into direct physical contact with exposed skin, minimizing the risk of allergic reactions to the PEDOT-Cl coating (although we note that this vapor-printed polymer was previously reported to be biocompatible[38]). This architecture was devised such that we could take advantage of the low lateral thermal conductivity of fabrics to maintain a heat gradient across the length of the thermopile even if a user continuously wears the knitted band for long periods.

The thermovoltages produced when multiple lab members wore this TEG band on their wrist, palm, or upper arm were recorded using a multimeter. The TEG band displayed well-behaved thermoelectric behavior when worn on the hand (the thermopile was centered on the palm), with approximately similar voltage outputs (≈10 mV) produced indoors for multiple users over multiple wears. However, random voltage fluctuations caused by varying thermal contact between the wearer and the TEG were inevitably observed when the band was worn on either the wrist or the upper arm and, especially, if the wearer was mobile and/or exercising. In contrast, palms provided consistent thermal contact with the knit band, even during periods of high exertion and mobility. This finding reveals the complex set of variables that need to be taken into account when designing a wearable TEG and emphasizes the need for the TEG to be in tight, unchanging contact with specific parts of the body in order to provide the highest possible thermopower outputs.[37]

Figure 3e plots the thermovoltage outputs created when multiple volunteers wore ten different TEG bands on the palm of their hand and either remained indoors in an office environment (T_C = 25 °C) or stood outdoors on a cold day (T_C = 2 °C). In this graph, the *x*-axis corresponds to the difference in temperature between the subject's palm and the ambient air. Although subject-to-subject variations in voltage output were noted, little batch-to-batch variation was observed when the same user wore different TEG bands. Substantially higher output voltages were achieved from the knitted TEG band when the palm of various volunteers was used as a heat source, as compared to the measured voltage output of its constituent cotton fabric thermopile with temperature-controlled copper blocks.

Perspiration significantly increased the thermovoltage output of the TEG armband. The subject with perspiration on their palm produced a voltage output of up to 24 mV, while the next closest output was 10 mV for a subject with dry palms. Damp cotton is known to possess a higher thermal conductivity than dry cotton[34] and, therefore, we attribute such an increase in TEG efficiency to improved heat transfer from the body to the fabric thermopile when the wearer is sweating. This observation bodes well for the applicability of all-fabric wearable TEGs, as these devices are often invoked as backup energy generators for activity tracking devices.[3–8] We could also "turn off" heat transfer from the body to the thermopile by inserting various plastic thermal reflectance layers between a wearer's wrist and the TEG band (Figure 3f). A thin cling-wrap insert attenuated the observed thermovoltage output from a TEG band, whereas a thick neoprene glove effectively annihilated the thermovoltage, again emphasizing the importance of tight, sustained thermal contact between the body and a wearable TEG.

3. Conclusion

Wearable thermoelectric generators face unique challenges because of extra demands for biocompatibility, flexibility, mechanical stability, and low operating temperatures. Known iterations of body-mounted thermopiles have large form factors, contain expensive or toxic materials with low elemental abundance, and quickly reach thermal equilibrium with a human body, meaning that thermoelectric power can only be generated over a short period of wear.

Here, we created an all-fabric thermopile by vapor printing persistently PEDOT-Cl onto commercial cotton fabrics. We showed that the reactive vapor coating process creates mechanically rugged conductive coatings that yield notably high efficiency fabric thermopiles, as compared to solution-processed counterparts. The vapor-coated cotton fabric reported here has the highest thermoelectric efficiency of a solely *p*-type conducting fabric to date, with a thermopower factor of 0.48 µW m^{-1} K^{-2} and a Seebeck coefficient of 16 µV K^{-1}, outperforming previously reported champions.[23]

Additionally, we described an approach to incorporate fabric thermopiles into garments that took advantage of the negligible lateral heat transfer across a swatch of woven cotton. A thick-knit wool band insulated part of the fabric thermopile from radiant body heat, ensuring that a temperature gradient could always be maintained across a rectangular thermopile, even when worn for long periods of time. Our all-fabric thermoelectric band afforded stable thermovoltage outputs as high as 23 mV when worn on the hand.

4. Experimental Section

Materials: 3,4-ethylenedioxythiophene (>98.0%) was purchased from TCI. Iron(III) chloride (97%), poly(3,4-ethylenedioxythiophene)-poly(styrenesulfonate) (1.1% in H_2O), and silver conductive paste (≥75%) were purchased from Sigma-Aldrich. Methanol (≥99.8%) and hydrochloric acid (36.5–38.0% w/w) were purchased from Fisher Scientific. All chemicals were used without further purification. Silver plated (76%) nylon (24%) was purchased from Less EMF Inc. Carbon fibers were obtained from dismantling graphitized spun yarn carbon fabrics obtained from Fuel Cell Earth.

Vapor Coating: Vapor-phase polymerization of EDOT was performed in a custom-built tube chamber, made of quartz and containing a single monomer side inlet. The temperatures of the heating zones were controlled through resistive heating tape. The monomer was vaporized from a glass ampule and the oxidant from a tungsten crucible, and the distance of the sample from the monomer inlet was 5 in. for all depositions. The process pressure for depositions was maintained between 150 and 200 mTorr. All samples reported were deposited on raw, natural textiles. The PEDOT-Cl was obtained using $FeCl_3$ as an oxidant, and a sequential heating algorithm was followed. First the monomer, substrate, and oxidant zones were heated at 80, 80, and 170 °C, respectively, for 10 min. Second, the monomer inlet was opened, and the vapors were introduced into the tube, allowing the polymerization reaction to proceed for 15 min to obtain a film thickness of 1 µm. Film thickness values were obtained using optical profilometry on a silicon test coupon that was coated simultaneously with the fabrics. After the deposition, samples were rinsed with copious amounts of methanol and 1% vol hydrochloric acid to remove residual monomer and oxidant and allowed to dry in ambient conditions. When washing PEDOT-Cl coated fabrics for durability tests, the samples were added to water with a Gain detergent pod and stirred/heated to 50 °C. PEDOT:PSS was drop cast onto cotton, dried in ambient conditions for 1 h, then annealed at 100 °C for 1 h. This process was repeated five times to increase the loading of PEDOT:PSS and obtain highly conductive films.

Thermoelectric Characterization: An in-house setup was used to measure the Seebeck coefficients, power factors, and conductivities. Fabric swatches were cut into 1.5 cm × 1.5 cm squares. These samples were positioned evenly across two copper blocks, one of which was heated. A Keithley 2440 5A sourcemeter was used to measure the conductivity through a four-point probe, and a Keithley 2182A Nanovoltmeter was used to record the output voltages.

The Seebeck coefficient was calculated using Equation (1)

$$S = \left(\frac{dV}{dT}\right)_{I=0} \tag{1}$$

Conductivity was calculated using Equation (2)

$$\sigma = G\left(\frac{l}{w \cdot t}\right) \tag{2}$$

where G is the slope of the IV curve, l is the distance between the probes (1.1 cm), w is the width of the sample, and t is the thickness of the coating. The thickness was measured from the polymer coating on a glass slide, which was placed next to the fabric during each deposition. For the PEDOT-Cl coating, a coating thickness of 1 µm was assumed and no further considerations for sample geometry were taken into account. For the PEDOT:PSS sample, cross-sectional SEMs clearly revealed the penetration depth of the PEDOT:PSS into the fabrics and this penetration depth was considered to be the coating thickness.

Power factor was calculated using Equation (3)

$$PF = S^2 \sigma \tag{3}$$

Thermopile Fabrication: Using a polyimide tape mask, PEDOT-Cl was deposited on textiles in two rectangles, 45 mm long and 5 mm wide, with a spacing of 5 mm. Carbon fibers of 45–50 mm in length were sewed onto the coated fabric such that two opposite ends of the PEDOT-Cl legs were connected together. Cotton thread was used to sew silver nylon squares onto the ends of each leg and embroider on the carbon fibers. For the wearable devices, the band was knit in-house using Lion brand acrylic (100%) yarn and the devices were sewn on using cotton thread.

Thermopile Characterization: Thermoelectric properties of devices were characterized in a custom-built setup, using copper blocks (2 in. × 2 in. × 2 in.), one held at room temperature (25 °C) and the other controllably heated using an OptiMag hot plate with a temperature probe. Blocks were positioned with 1 in. of space between them. All output measurements were taken by connecting the probes of a FLUKE 27 II multimeter to the electrodes on the device. Body mounted device outputs were measured using alligator clips attached to the probes, taking care to prevent the contact of the metal clip with the skin to avoid false readouts.

Supporting Information

Supporting Information is available from the Wiley Online Library or from the author.

Acknowledgements

Conflict of Interest

The authors declare no conflict of interest.

Keywords

[1] S. Patel, H. Park, P. Bonato, L. Chan, M. Rodgers, *J. Neuroeng. Rehabil.* **2012**, *9*, 21.
[2] T. Hughes-Riley, T. Dias, C. Cork, *Fibers* **2018**, *6*, 34.
[3] P. Xiong, H. Weiguo, Z. L. Wang, *Small* **2017**, *14*, 1702817.
[4] F. F. Ru, T. Wei, Z. L. Wang, *Adv. Mater.* **2016**, *28*, 4283.
[5] M. K. Kim, M. S. Kim, S. E. Jo, H. L. Kim, S. M. Lee, Y. J. Kim, in *2013 Transducers Eurosensors XXVII: The 17th Int. Conf. on Solid-State Sensors, Actuators and Microsystems (TRANSDUCERS EUROSENSORS XXVII)*, IEEE, Barcelona, Spain **2013**, 1376–1379.
[6] M. K. Kim, M. S. Kim, S. Lee, C. Kim, Y. J. Kim, *Smart Mater. Struct.* **2014**, *23*, 105002.
[7] S. J. Kim, H. We, B. J. Cho, *Energy Environ. Sci.* **2014**, *7*, 1959.
[8] M. Hyland, H. Hunter, J. Liu, E. Veety, D. Vashaee, *Appl. Energy* **2016**, *182*, 518.
[9] O. Bubnova, X. Crispin, *Energy Environ. Sci.* **2012**, *5*, 9345.
[10] S. Peng, D. Wang, J. Lu, M. He, C. Xu, Y. Li, S. Zhu, *J. Polym. Environ.* **2017**, *25*, 1208.
[11] B. Russ, A. Glaudell, J. J. Urban, M. L. Chabinyc, R. A. Segalman, *Nat. Rev. Mater.* **2016**, *1*, 16050.
[12] G. J. Snyder, E. S. Toberer, *Nat. Mater.* **2008**, *7*, 105.

[13] V. Leonov, *IEEE Sens. J.* **2013**, *13*, 2284.

[14] A. R. M. Siddique, S. Mahmud, B. V. Heyst, *Renewable Sustainable Energy Rev.* **2017**, *73*, 730.

[15] Z. Wang, V. Leonov, P. Fiorini, C. van Hoof, *Sens. Actuators, A* **2009**, *156*, 95.

[16] S. K. Yee, N. E. Coates, A. Majumdar, J. J. Urban, R. A. Segalman, *Phys. Chem. Chem. Phys.* **2013**, *15*, 4024.

[17] Z. Lu, H. Zhang, C. Mao, C. M. Li, *Appl. Energy* **2016**, *164*, 57.

[18] L. Francioso, C. De Pascali, I. Farella, C. Martucci, P. Creti, P. Siciliano, A. Perrone, in *2010 IEEE Sensors* IEEE, Kona, HI **2010**, 747.

[19] Z. Cao, E. Koukharenko, M. J. Tudor, R. N. Torah, S. P. Beeby, *J. Phys.: Conf. Ser.* **2013**, *476*, 012031.

[20] C. Zhou, C. Dun, Q. Wang, K. Wang, Z. Shi, D. L. Carroll, G. Liu, G. Qiao, *ACS Appl. Mater. Interfaces* **2015**, *7*, 21015.

[21] Rare Earth Elements—Critical Resources for High Technology | USGS Fact Sheet 087-02, https://pubs.usgs.gov/fs/2002/fs087-02/ (accessed: June **2018**).

[22] V. Leonov, *J. Micromech. Microeng.* **2011**, *21*, 125013.

[23] Y. Du, K. Cai, S. Chen, H. Wang, S. Z. Shen, R. Donelson, T. Lin, *Sci. Rep.* **2015**, *5*, 6411.

[24] M. Orrill, S. LeBlanc, *J. Appl. Polym. Sci.* **2017**, *134*, 44256.

[25] S. N. Patel, M. L. Chabinyc, *J. Appl. Polym. Sci.* **2017**, *134*, 44403.

[26] J. D. Ryan, A. Lund, A. I. Hofmann, R. Kroon, R. Sarabia-Riquelme, M. C. Weisenberger, C. Müller, *ACS Appl. Energy Mater.* **2018**, *1*, 2934.

[27] Y. Chen, Y. Zhao, Z. Liang, *Energy Environ. Sci.* **2015**, *8*, 401.

[28] C. Cho, K. L. Wallace, P. Tzeng, J.-H. Hsu, C. Yu, J. C. Grunlan, *Adv. Energy Mater.* **2016**, *6*, 1502168.

[29] C. A. Hewitt, A. B. Kaiser, S. Roth, M. Crapsl, R. Czerwl, D. L. Carroll, *Nano Lett.* **2012**, *12*, 1307.

[30] L. K. Allison, S. Hoxie, T. L. Andrew, *Chem. Commun.* **2017**, *53*, 7182.

[31] N. Cheng, T. L. Andrew, *J. Visualized Exp.* **2018**, *131*, e56775.

[32] T. L. Andrew, L. Zhang, N. Cheng, M. Baima, J. J. Kim, L. K. Allison, S. Hoxie, *Acc. Chem. Res.* **2018**, *51*, 850.

[33] T. Bashir, M. Skrifvars, N. K. Persson, *Polym. Adv. Technol.* **2011**, *22*, 2214.

[34] E. S. Rood, *Phys. Rev.* **1921**, *18*, 356.

[35] P. M. Smith, L. Su, W. Gong, N. Nakamura, B. Reeja-Jayan, S. Shen, *RSC Adv.* **2018**, *8*, 19348.

[36] Y. Guo, M. T. Otley, M. Li, X. Zhang, S. K. Sinha, G. M. Treich, G. A. Sotzing, *ACS Appl. Mater. Interfaces* **2016**, *8*, 26998.

[37] Y. S. Chen, J. Fan, X. Qian, W. Zhang, *Text. Res. J.* **2004**, *74*, 742.

[38] L. Zhang, M. Baima, T. L. Andrew, *ACS Appl. Mater. Interfaces* **2017**, *9*, 32299.